CWP-919

Localized time-lapse full-waveform inversion

Colton Kohnke and Paul Sava

Center for Wave Phenomena, Colorado School of Mines

ABSTRACT

Full waveform inversion of seismic data requires building the gradient of an objective function from simulated forward and adjoint wavefields to update the model. After each model update, wavefields need to be recomputed for the next iteration. Typical models are large and computing wavefields is computationally expensive. For time-lapse applications, the model is expected to change only in a local region, therefore much of the computing time is wasted in regions where the model does not need updating. The technique described in this paper outlines a process to localize the forward and adjoint wavefield propagation to a local domain such that the wavefields simulated locally are exact compared with those simulated in the full domain. The gradient of the objective function is also accurately built inside the local domain. The wavefields and gradient at each iteration are computed locally at a cost orders of magnitude lower than in the full domain, enabling more computationally efficient inversions. Wavefield localization facilitates more efficient FWI, while also constraining model updates to the local domain.

Key words: 4C, 4D, computational efficiency, localization, FWI

1 INTRODUCTION

As geophysical problems get larger, our ability to compute solutions efficiently depends on computation speed, and computational efficiency. While the first factor depend primarily on hardware advances, the second is more problem-dependent. An example is time-lapse full waveform inversion (FWI) (Virieux and Operto, 2009; Tarantola, 1984; Symes, 2007; Pratt, 1999). In this problem, seismic surveys are repeated multiple times, typically after injection or production, followed by iterative inversion to infer model changes between the baseline and subsequent surveys. The model update at each waveform inversion iteration is computed from the gradient of an objective function, which is simply the cross-correlation of forward and adjoint wavefields, as in reverse-time migration. The adjoint wavefield is computed using the data difference at the receivers as its source term. After each model update, the forward and adjoint wavefields must be recomputed to build the gradient for the next model update. In general, these models are large and computing wavefields is expensive. This problem is further exaggerated by the fact that for time-lapse applications the model is expected to change in a localized region of interest, and therefore much of the time spent simulating waves is wasted.

The technique described in this paper outlines a process to localize wavefield propagation and build FWI gradients inside a small domain at lower computational cost than using the full model. This is accomplished by using localization techniques (Vasmel and Robertsson, 2016; Broggini et al., 2017; Willemsen et al., 2016) that essentially move the sources and receivers to the local domain of interest by assembling an equivalent localized experiment. Boundary conditions on the local domain are applied such that wavefields simulated cheaply in the local domain are the same as if they were computed using the full computational domain. The computational domain is thus restricted to the space of interest, making wavefields simulations less expensive.

Techniques for acoustic wavefield localization are introduced by van Manen et al. (2007) who explore perturbed scattering problems to show exact reconstruction in a local domain. Vasmel and Robertsson (2016) and Broggini et al. (2017) expand the theory with time-domain boundary condition on the local domain to exactly reproduce interior wavefields and show applications to seismic imaging. Willemsen et al. (2016) and Willemsen and Malcolm (2016) show boundary conditions in the frequency domain and FWI applied to updating salt boundaries. Time-lapse FWI in the frequency domain is discussed by Malcolm and Willemsen (2016). In this paper we show how the forward and adjoint wavefields can be localized in the time-domain, and how local gradients are built for accelerated time-lapse FWI. Reverse-time migration follows a similar process to building FWI gradients and benefits from wavefield localization.

Similar theory for localization exists for both elastic and

electromagnetic waves, meaning that localized inversion for these methods is also possible. Since all time-varying (acoustic, elastic, and electromagnetic) field methods can be solved locally using finite-differences, other computationally expensive processes, such as joint time-lapse inversion of seismic and electromagnetic data, can be explored in a local domain.

2 THE VECTOR-ACOUSTIC OPERATOR

Modeling seismic data is a game of tradeoffs. In an ideal world, one would use the most accurate elastic wave equation solver to simulate wavefields in a model. However, this process is computationally expensive and the number of needed model parameters grows with increasing model complexity. Inversion using the elastic wave equation is costly and needs to recover a multitude of physical properties. In isotropic media, one can employ an acoustic wave equation solver as an approximation to the elastic wave equation. This approximation loses the sensitivity to elastic properties, but gains computational speedup as wavefield simulations in acoustic media are significantly faster than in elastic. The number of model parameters recovered for acoustic inversion is also significantly smaller.

Standard marine seismic acquisition systems record only the acoustic pressure wavefield. However, recent technology advancements in marine seismic acquisition allows for the recording of vector acoustic seismic data, comprised of both pressure and particle velocity wavefields (Robertsson et al., 2008). The systems are also capable of using monopole and dipole sources (Halliday et al., 2012). Having access to vector acoustic wavefields provides opportunities to improve both reverse-time migration (RTM) depth-imaging and full waveform inversion (FWI) (Fleury and Vasconcelos, 2013). To model wavefields produced by these systems one must use the first order vector-acoustic wave equation, as discussed next.

To confine wavefields to a local domain, the pressure and particle velocity on the boundary of the domain needs to be computed. To accomplish this, we consider the first order vector-acoustic wave equations

$$\rho \frac{\partial \mathbf{v}}{\partial t} + \nabla p = \mathbf{f} \tag{1}$$

$$\frac{1}{\rho c^2}\frac{\partial p}{\partial t} + \nabla \cdot \mathbf{v} = q, \tag{2}$$

which couple the particle velocity $\mathbf{v}(\mathbf{x},t)$ with the pressure $p(\mathbf{x},t)$ reconstructed from dipole $\mathbf{f}(\mathbf{x},t)$ and monopole $q(\mathbf{x},t)$ sources. The wavefields propagate in a medium with spatially variable density $\rho(\mathbf{x})$ and velocity $c(\mathbf{x})$. The vector-acoustic equations are solved iteratively using finite-differences on a staggered grid in space and time, similar to a Yee lattice in electromagnetics (Yee, 1966). Implementing the staggering in space and time greatly increases the numerical stability of the system compared to the second order wave equation at the cost of computing an additional wavefield variable ($\mathbf{v}$) at each time step. The pressure sits on the main grid at integer time steps and the particle velocity is shifted in space and exists at half time steps. The equations are solved in a leapfrog scheme: particle velocity is derived from the preceding pressure, and pressure is derived from the preceding particle velocity. A layout of the pressure and particle velocity grids is shown in Figure 1. The black grid is for pressure and the blue and green grids are for particle velocity. The latter grids are shifted in space by their respective offsets and exist half a time step ahead of the pressure grid. The monopole q source term exists at half time steps, at the same times as the particle velocity grids. The dipole $\mathbf{f}$ source term exists at full time steps with the pressure grid.

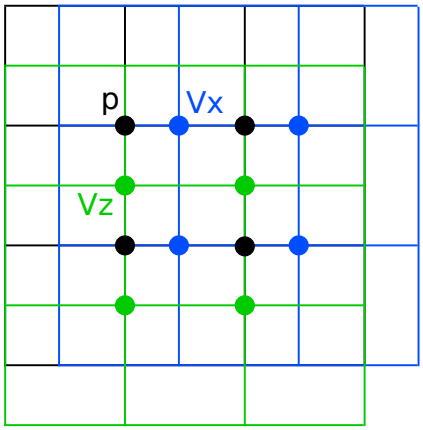


Figure 1. 2D finite-difference grids for equation 1. The pressure grid is shown in black. The grid for the x-component of particle velocity is shown in blue and is shifted by $dx/2$. The z-component of particle velocity is shown in green and is shifted by $dz/2$. In 3D, the y-component of particle velocity is shifted by $dy/2$. Furthermore, the particle velocity grids are shifted from the pressure grid in time by $dt/2$.

We can use the system of equations 1 and 2 to define a linear operator $\mathbf{L}$ linking source wavefield $\mathbf{w}_s(\mathbf{x},t)$, and data at the source locations $\mathbf{d}_s(t)$

$$\mathbf{L}\mathbf{w}_s = \mathbf{d}_s. \tag{3}$$

The forward wave propagation operator $\mathbf{L}$, source wavefield $\mathbf{w}_s(\mathbf{x},t)$, and data at the source locations $\mathbf{d}_s(t)$ are defined as

$$\mathbf{L} = \left[\begin{array}{cccc|ccc} \frac{\rho}{\Delta t} & 0 & 0 & \dots & \mathbf{G} & 0 & 0 & \dots \\ -\frac{\rho}{\Delta t} & \frac{\rho}{\Delta t} & 0 & \dots & 0 & \mathbf{G} & 0 & \dots \\ 0 & -\frac{\rho}{\Delta t} & \frac{\rho}{\Delta t} & \dots & 0 & 0 & \mathbf{G} & \dots \\ \vdots & \vdots & \vdots & \ddots & \vdots & \vdots & \vdots & \ddots \\ \hline \mathbf{D} & 0 & 0 & \dots & \frac{1}{\rho c^2 \Delta t} & 0 & 0 & \dots \\ 0 & \mathbf{D} & 0 & \dots & -\frac{1}{\rho c^2 \Delta t} & \frac{1}{\rho c^2 \Delta t} & 0 & \dots \\ 0 & 0 & \mathbf{D} & \dots & 0 & -\frac{1}{\rho c^2 \Delta t} & \frac{1}{\rho c^2 \Delta t} & \dots \\ \vdots & \vdots & \vdots & \ddots & \vdots & \vdots & \vdots & \ddots \end{array}\right], \tag{4}$$

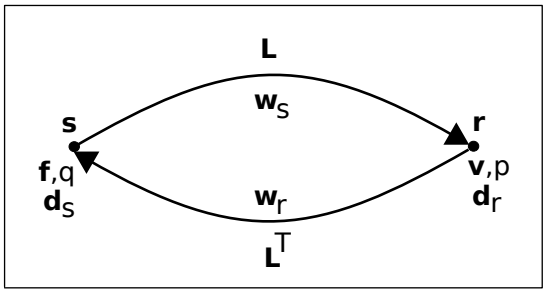


Figure 2. Visual representation of the forward and adjoint operators in the full domain. The forward operator $\mathbf{L}$ creates the source wavefield $\mathbf{w}_s$ from the data $\mathbf{d}_s$ at the source $\mathbf{s}$, and is measured at the receivers $\mathbf{r}$. The adjoint creates the adjoint wavefield $\mathbf{w}_r$ from the data $\mathbf{d}_r$ at the receivers $\mathbf{r}$ and is measured at the sources $\mathbf{s}$.

$$\mathbf{w}_s = \begin{bmatrix} \mathbf{v}_0 \\ \mathbf{v}_1 \\ \mathbf{v}_2 \\ \vdots \\ \hline p_0 \\ p_1 \\ p_2 \\ \vdots \end{bmatrix}, \text{ and } \mathbf{d}_s = \begin{bmatrix} \mathbf{f}_0 \\ \mathbf{f}_1 \\ \mathbf{f}_2 \\ \vdots \\ \hline q_0 \\ q_1 \\ q_2 \\ \vdots \end{bmatrix}. \tag{5}$$

Numeral subscripts in $\mathbf{w}_s$ and $\mathbf{d}_s$ denote the timestep. $\mathbf{G}$ is the gradient operator (∇) and $\mathbf{D}$ is the divergence operator ($\nabla\cdot$). The gradient operator performs spatial derivatives on pressure and shifts information spatially from the pressure grid to the particle velocity grid. The divergence operator performs spatial derivatives on particle velocity and shifts information spatially from the velocity grid to the pressure grid. The top left and bottom right blocks on $\mathbf{L}$ perform the finite-difference time derivative of the particle velocity and pressure wavefields. These derivates allow for temporal movement from pressure to particle velocity (bottom right) and particle velocity to pressure (top left). Through these operations, all quantities are placed on the correct grids as required by the wave equations 1 and 2. The system in equation 3 is solved forward in time for $\mathbf{w}_s$ starting with the first particle velocity time step $\mathbf{v}_0$, then p_0, $\mathbf{v}_1$, p_1, etc. The resulting wavefield $\mathbf{w}_s$ is the state variable needed for waveform inversion. The data this wavefield produces at receiver locations $\mathbf{d}_r(t)$ is found by spatially restricting the wavefield to the receivers. Figure 2 depicts how forward problem is solved. The source term $\mathbf{d}_s$ is injected at the source location and is propagated forward in time using $\mathbf{L}$, producing the source wavefield $\mathbf{w}_s$. The wavefield $\mathbf{w}_s$ is saved at the receiver locations to produce $\mathbf{d}_r$.

The adjoint wavefield is found using the adjoint modeling operator

$$\mathbf{d}_r = \mathbf{L}^\dagger \mathbf{w}_r \tag{6}$$

to solve for the adjoint wavefield $\mathbf{w}_r$ given the data at the receiver locations. $\mathbf{L}^\dagger$ is the adjoint of the wave propagation operator $\mathbf{L}$ and is defined as

$$\mathbf{L}^\dagger = \left[\begin{array}{cccc|ccc|c} \frac{\rho}{\Delta t} & -\frac{\rho}{\Delta t} & 0 & \dots & \mathbf{D}^\dagger & 0 & 0 & \dots \\ 0 & \frac{\rho}{\Delta t} & -\frac{\rho}{\Delta t} & \dots & 0 & \mathbf{D}^\dagger & 0 & \dots \\ 0 & 0 & \frac{\rho}{\Delta t} & \dots & 0 & 0 & \mathbf{D}^\dagger & \dots \\ \vdots & \vdots & \vdots & \ddots & \vdots & \vdots & \vdots & \ddots \\ \hline \mathbf{G}^\dagger & 0 & 0 & \dots & \frac{1}{\rho c^2 \Delta t} & -\frac{1}{\rho c^2 \Delta t} & 0 & \dots \\ 0 & \mathbf{G}^\dagger & 0 & \dots & 0 & \frac{1}{\rho c^2 \Delta t} & -\frac{1}{\rho c^2 \Delta t} & \dots \\ 0 & 0 & \mathbf{G}^\dagger & \dots & 0 & 0 & \frac{1}{\rho c^2 \Delta t} & \dots \\ \vdots & \vdots & \vdots & \ddots & \vdots & \vdots & \vdots & \ddots \end{array}\right]. \tag{7}$$

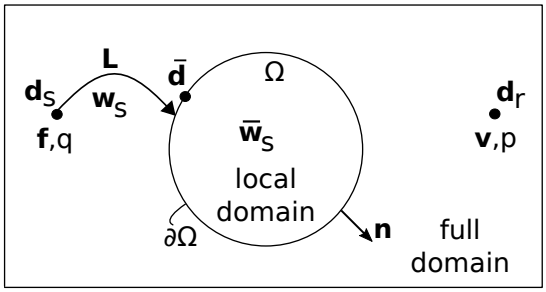
$\mathbf{D}^\dagger$ and $\mathbf{G}^\dagger$ are the adjoint of the corresponding operators. $\mathbf{D}^\dagger$ describes the negative gradient operator ($-\nabla$) and $\mathbf{G}^\dagger$ describes the negative divergence operator ($-\nabla\cdot$). This system is solved for the adjoint $\mathbf{w}_r$ wavefields in reverse time, starting with q_N, then for $\mathbf{f}_N$, q_{N-1}, $\mathbf{f}_{N-1}$, etc. The receiver wavefield (the adjoint state variable) is restricted spatially to obtain the data at the source $\mathbf{d}_s$.

The forward and adjoint wavefields can be used to solve tomographic problems using the adjoint-state method Plessix (2006); Tromp et al. (2004); Fichtner and Trampert (2011), which is an efficient way of computing model gradients. In this method the state variable (the forward wavefield $\mathbf{w}_s$) is computed using equation 3. The adjoint source is derived by taking the difference between the observed and predicted wavefields at the receiver locations ($\mathbf{d}_r = \mathbf{d}_r^{\text{obs}} - \mathbf{d}_r^{\text{pre}}$). The adjoint source is used to create the adjoint variable (the adjoint wavefield $\mathbf{w}_r$) using equation 6. The gradient of the model, which can be used for FWI, is the zero-lag crosscorrelation of the state and adjoint variables. The gradient requires two wavefield simulations, one for each state variable at every iteration, which can be computationally expensive depending on the size of the model.

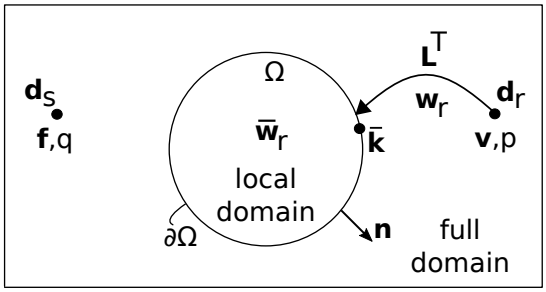
3 WAVEFIELD LOCALIZATION

In 4D FWI, the model is expected to change in a localized region of interest due to a known production or injection event. This means that much of the time spend computing the forward and adjoint wavefields is in a portion of the model that does not change between model updates. It is significantly more efficient to localize the wavefields to the region of interest, with the constraint that the waves that propagate inside the local region are the same as the waves simulated in the full domain.

Consider the schematic geometry in Figure 3. Using equations equation 3 and 6 we can compute the forward and adjoint wavefields between the sources and receivers and obtain a gradient to update the model. Assuming that perturbations only occur in the region Ω, we can simulate wavefields from data recorded on $\partial\Omega$ using Rayleigh's Reciprocity Theorem (de Hoop, 1995; Vasmel and Robertsson, 2016):



(a)



(b)

Figure 3. Localization process for the (a) source and (b) receivers. On the source side, the data at the source $\mathbf{d}_s$ is propagated using $\mathbf{L}$ and measured on $\partial\Omega$. The local source term $\bar{\mathbf{d}}$ is derived on $\partial\Omega$ and propagated using $\mathbf{L}$ to produce the local source wavefield $\bar{\mathbf{w}}_s$. On the receiver side, the data at the receiver $\mathbf{d}_r$ is propagated using $\mathbf{L}^\dagger$ and measured on $\partial\Omega$. The local adjoint source term $\bar{\mathbf{k}}$ is derived on $\partial\Omega$ and propagated using $\mathbf{L}^\dagger$ to produce the local adjoint wavefield $\bar{\mathbf{w}}_r$.

$$p = \oint_{\partial\Omega} [p_A * \mathbf{v}_B - \mathbf{v}_A * p_B]\mathbf{n} dS = \tag{8}$$

$$\int_\Omega [p_A * q_B - \mathbf{v}_A * \mathbf{f}_B - q_A * p_B + \mathbf{f}_A * \mathbf{v}_B] dV. \tag{9}$$

The symbol $*$ denotes temporal convolution. Rayleigh's Reciprocity Theorem links the acoustic states, A and B, of a region Ω bounded by $\partial\Omega$ with outward pointing normal $\mathbf{n}$. The acoustic states can have different source terms inside Ω, but as long as the wavefields on the boundary are known, the wavefields inside the region can be computed. If we replace the B acoustic state source terms with the Green's function, we obtain

$$p = \oint_{\partial\Omega} [p * G^{\mathbf{f}} + \mathbf{v} * G^q] \cdot \mathbf{n} dS \tag{10}$$

as the boundary condition to reconstruct the wavefields inside Ω (Broggini et al., 2017). G is the Green's function, where the superscript denotes the source type. The left-hand side represents the pressure at any location inside Ω, and the right-hand side values exist on the boundary. The Green's function acts as a propagator that moves energy from the boundary to the inside of the domain, and can be replaced with weighted source terms on the boundary. $G^{\mathbf{f}}$ is replaced with dipole sources weighted by $p\mathbf{n}$ and G^q is replaced with monopole sources weighted by $\mathbf{v} \cdot \mathbf{n}$. Therefore, equation 10 states that if the pressure p and particle velocity $\mathbf{v}$ wavefields are known on $\partial\Omega$ in the full domain, the $\partial\Omega$ sources q and $\mathbf{f}$ can be derived such that the localized pressure and particle velocity wavefields are equivalent to those computed in the full domain. The sources on $\partial\Omega$ are

$$\begin{aligned} \mathbf{f}_{\partial\Omega} &= p_{\partial\Omega}\mathbf{n} \\ q_{\partial\Omega} &= \mathbf{v}_{\partial\Omega} \cdot \mathbf{n}. \end{aligned} \tag{11}$$

We can also write the new localized source term on $\partial\Omega$ as

$$\bar{\mathbf{d}}_{\partial\Omega} = \mathbf{N}\mathbf{d}_{\partial\Omega}. \tag{12}$$

The operator $\mathbf{N}$ acts on $\mathbf{d}_{\partial\Omega}$, the measured data on $\partial\Omega$ in the full domain, to produce the localized source terms $\bar{\mathbf{d}}_{\partial\Omega}$ on $\partial\Omega$. Our convention is that the overbar denotes derived terms that are used for localization, whereas the subscript denotes where the quantity exists. Therefore, the operator $\mathbf{N}$ is defined as

$$\mathbf{N} = \begin{bmatrix} 0 & \mathbf{n} \\ \mathbf{n}\cdot & 0 \end{bmatrix} \tag{13}$$

Localizing the adjoint wavefield mirrors the forward. We simulate the adjoint wavefield by time reversal and capture it on $\partial\Omega$ to get the adjoint source terms $\mathbf{k}_{\partial\Omega}$. Therefore, the new adjoint sources are

$$\mathbf{N}\mathbf{k}_{\partial\Omega} = \bar{\mathbf{k}}_{\partial\Omega}. \tag{14}$$

Here $\mathbf{k}_{\partial\Omega}$ is the measured adjoint wavefields on $\partial\Omega$ in the full domain and $\bar{\mathbf{k}}_{\partial\Omega}$ is the new source term on $\partial\Omega$ necessary to simulate the adjoint wavefields in the local domain. Substituting the local forward and adjoint source terms into the forward and adjoint equations yields the linear system

$$\begin{aligned} \mathbf{L}\bar{\mathbf{w}}_s &= \bar{\mathbf{d}}_{\partial\Omega} \\ \bar{\mathbf{k}}_{\partial\Omega} &= \mathbf{L}^\dagger \bar{\mathbf{w}}_r \end{aligned} \tag{15}$$

required to solve for the localized forward $\bar{\mathbf{w}}_s$ and adjoint $\bar{\mathbf{w}}_r$ wavefields. By using the derived sources on the boundary of the local region, the wavefields inside the region will be unchanged, and are confined to a small region of the model, thus reducing computational cost considerably.

4 EXAMPLES

To illustrate this concept of localization, consider a $300 \times 200 \times 200$ gridpoint subset of the SEAM model and a 100^3 gridpoints subdomain centered around a 0.90km radius sphere (Ω), Figure 4. The large velocity model is the full domain and the region highlighted by the black circles form the smaller velocity model and the local domain. The local domain is an order of magnitude smaller than the full domain, which is in-

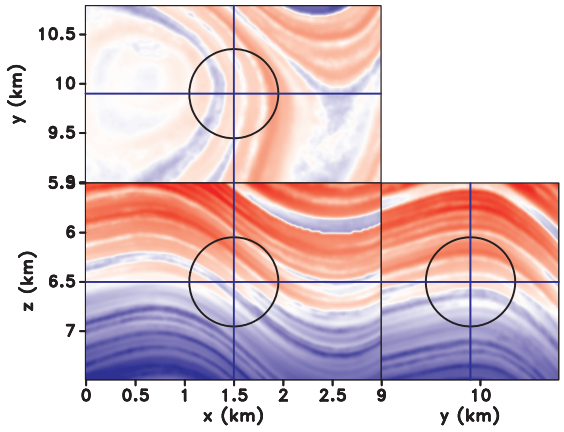


Figure 4. Subset of the SEAM velocity model used for the full domain simulations. The local domain boundary $\partial\Omega$ is highlighted in black.

dicative of an order of magnitude speedup for wavefield propagation.

Figure 5 shows the comparison of the forward operator in the full and local domains for the pressure wavefields. The wavefield reconstructed inside Ω matches the one computed in the full domain. Similarly, the adjoint pressure wavefields in the full and local domain are shown in Figure 6. The adjoint wavefields in the local domain also match inside the local domain as if they were computed in the full domain. The boundaries of the local domain cancel out the wavefields and confine them to propagating inside $\partial\Omega$ for both forward and the adjoint wavefields.

This process of wavefield localization relocates sources and receivers to an interior surface $\partial\Omega$ in a process similar to redatuming. The sources on $\partial\Omega$ are able to confine propagating waves to the small region; any outgoing waves are canceled out by these boundary sources. The derived forward and adjoint sources therefore form the boundary condition on Ω. If the velocity model inside Ω changes, the total wavefield propagates inside Ω and the boundary condition cancels out the wavefield that propagate in the original model (the background wavefield). We are then left with the scattered wavefield on $\partial\Omega$, which can be compared (subtracted) from the observed data relocated to $\partial\Omega$ to form the adjoint source. This implies that once the source and receiver wavefields are localized, we have access to all of the necessary information for FWI restricted to the domain Ω.

Consider a velocity model that has a perturbation confined to Ω, simulating the time-lapse change in the model (Figure 7). The gradient in the full domain is built by crosscorrelation of the forward $\mathbf{w}_s$ and adjoint $\mathbf{w}_r$ wavefields. In the local domain, the gradient is computed from the crosscorrelation of the local forward $\bar{\mathbf{w}}_s$ and adjoint $\bar{\mathbf{w}}_r$ wavefields. To compute the local adjoint source $\bar{\mathbf{k}}$ we relocate the observed data at the receiver to $\partial\Omega$ and take the data difference with the predicted wavefields on $\partial\Omega$. Once the observed and predicted wavefields are moved to $\partial\Omega$, the full domain can be ignored because the localized forward operator computes the scattered wavefield on $\partial\Omega$. Figure 8 shows the result of computing the pressure gradient in the full and the local domains. Since the wavefields are accurately localized, the gradients are also localized, and the full and local domain solutions match.

5 CONCLUSION

Time-lapse seismic FWI can be computationally expensive due to the size of the models used for wavefield propagation. We propose a method to localize the forward and adjoint wavefields required by FWI to compute gradients at significantly lower computational cost (orders of magnitude in 3D) in a local domain. The localization is enabled by boundary condition derived from Rayleigh's Reciprocity Theorem. The wavefields and gradients in the local domain match exactly their counterparts computed in the full model.

6 ACKNOWLEDGEMENTS

We thank the sponsors of the Center for Wave Phenomena, whose support made this research possible. The synthetic examples in this paper use the Madagascar open-source software package Fomel et al. (2013) freely available from `http://www.ahay.org`.

REFERENCES

Broggini, F., M. Vasmel, J. O. A. Robertsson, and D.-J. van Manen, 2017, Immersive boundary conditions: Theory, implementation, and examples: Geophysics, **82**, T97–T110.

de Hoop, A. T., 1995, Handbook of radiation and scattering of waves: Acoustic waves in fluids, elastic waves in solids, electromagnetic waves: Academic Press.

Fichtner, A., and J. Trampert, 2011, Hessian kernels of seismic data functionals based upon adjoint techniques: Geophysical Journal International, **185**, 775–798.

Fleury, C., and I. Vasconcelos, 2013, Adjoint-state reverse time migration of 4C data: Finite-frequency map migration for marine seismic imaging: Geophysics, **78**, WA159–WA172.

Fomel, S., P. Sava, I. Vlad, Y. Liu, and V. Bashkardin, 2013, Madagascar: open-source software project for multidimensional data analysis and reproducible computational experiments: Journal of Open Research Software, **1**, e8.

Halliday, D., J. O. A. Robertsson, I. Vasconcelos, D.-J. van Manen, R. Laws, K. Özdemir, and H. Grønaas, 2012, Full-wavefield, towed-marine seismic acquisition and applications: SEG Technical Program Expanded Abstracts 2012, Society of Exploration Geophysicists, 1–5.

Malcolm, A., and B. Willemsen, 2016, Rapid 4D FWI using a local wave solver: The Leading Edge, **35**, 1053–1059.

Plessix, R.-E., 2006, A review of the adjoint-state method for computing the gradient of a functional with geophysical applications: Geophysical Journal International, **167**, 495–503.

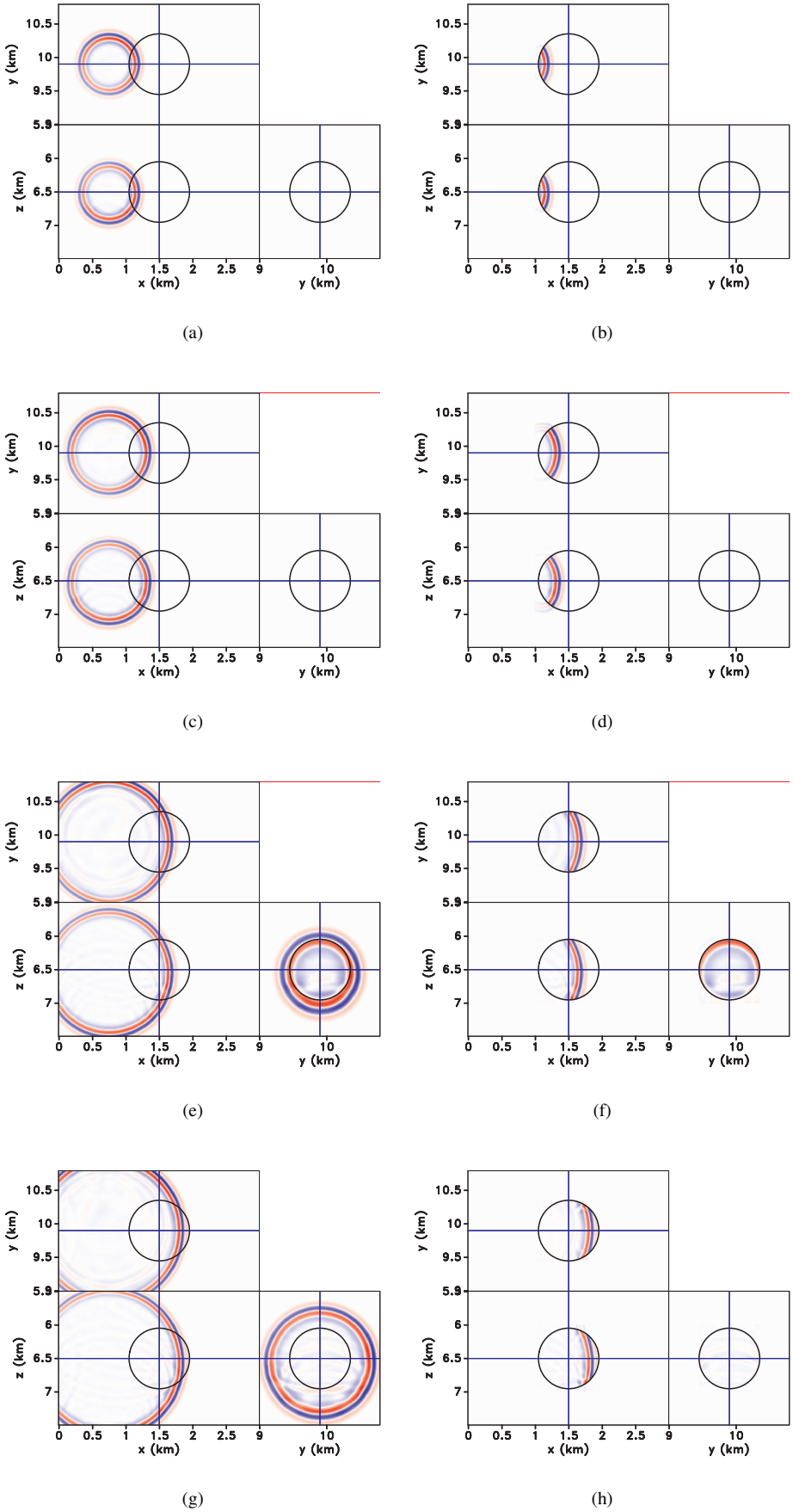


Figure 5. The forward pressure wavefields in the (left) full domain and (right) local domain.

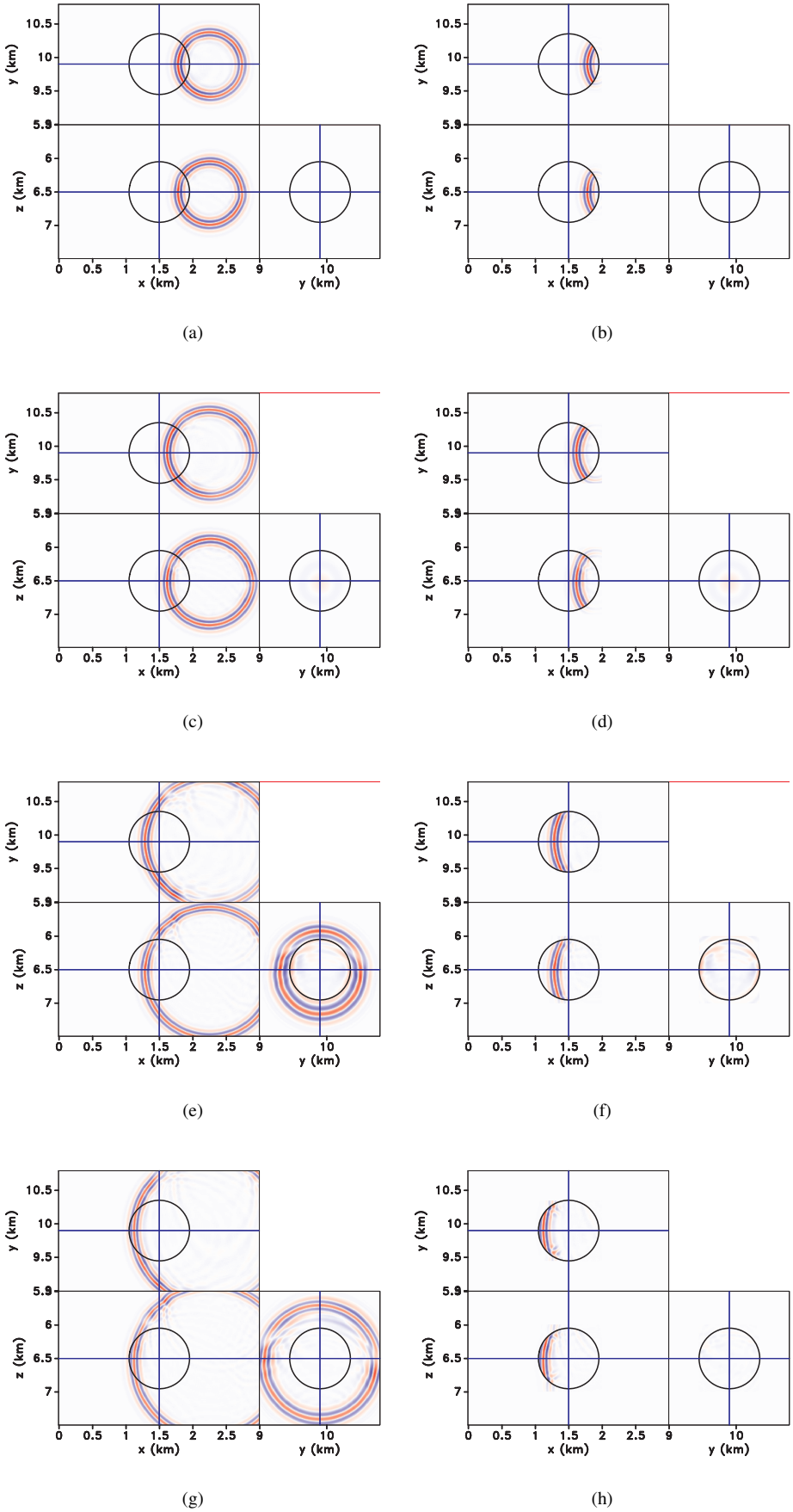


Figure 6. The adjoint pressure wavefields in the (left) full domain and (right) local domain.

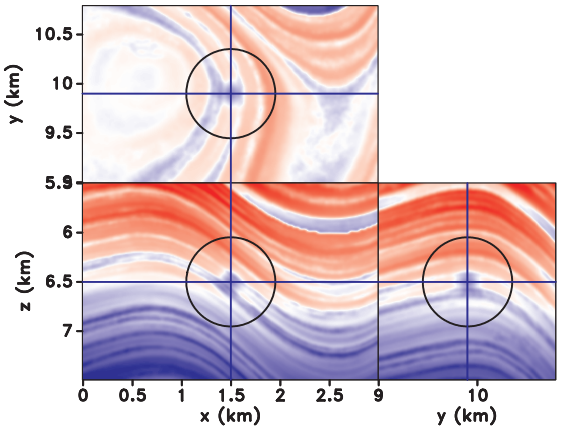
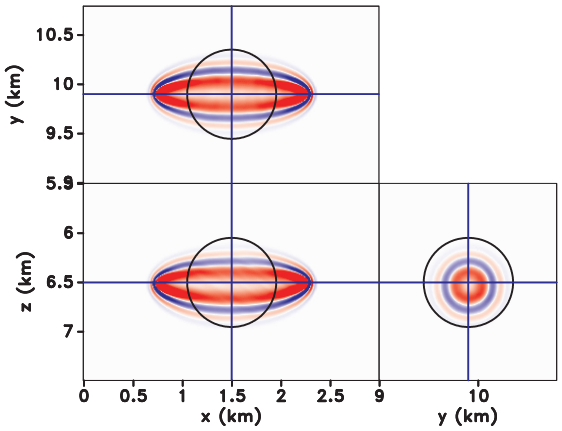
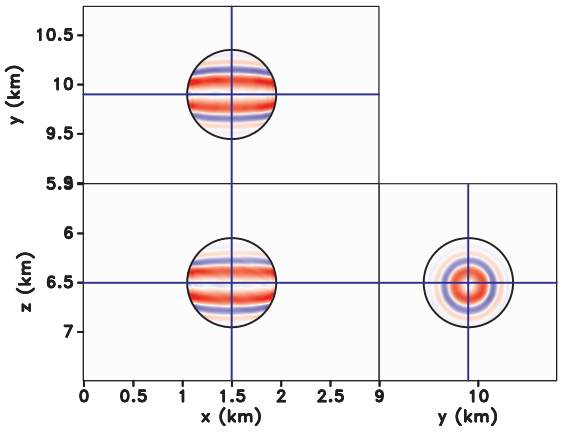


Figure 7. True velocity model for the construction of the observed wavefields at receivers. The boundary of the local domain is highlighted in black.



(a)



(b)

Figure 8. Gradient of objective function built from the crosscorrelation of forward and adjoint pressure wavefields in (a) the full domain and (b) the local domain.

Pratt, R. G., 1999, Seismic waveform inversion in the frequency domain, Part 1: Theory and verification in a physical scale model: Geophysics, **64**, 888–901.

Robertsson, J. O., I. Moore, M. Vassallo, K. Özdemir, D.-J. van Manen, and A. Özbek, 2008, On the use of multicomponent streamer recordings for reconstruction of pressure wavefields in the crossline direction: Geophysics, **73**, A45–A49.

Symes, W. W., 2007, Reverse time migration with optimal checkpointing: Geophysics, **72**, SM213–SM221.

Tarantola, A., 1984, Inversion of seismic reflection data in the Acoustic Approximation: Geophysics, **49**, 1259–1266.

Tromp, J., C. Tape, and Q. Liu, 2004, Seismic tomography, adjoint methods, time reversal and banana-doughnut kernels: Geophysical Journal International, **160**, 195–216.

van Manen, D.-J., J. O. A. Robertsson, and A. Curtis, 2007, Exact wave field simulation for finite-volume scattering problems: The Journal of the Acoustical Society of America, **122**, EL115–EL121.

Vasmel, M., and J. O. A. Robertsson, 2016, Exact wavefield reconstruction on finite-difference grids with minimal memory requirements: Geophysics, **81**, T303–T309.

Virieux, J., and S. Operto, 2009, An overview of full-waveform inversion in exploration geophysics: Geophysics, **74**, WCC1–WCC26.

Willemsen, B., and A. Malcolm, 2016, Coupling a local elastic solver to a background acoustic model to estimate phase variation: SEG Technical Program Expanded Abstracts 2016, Society of Exploration Geophysicists, 3945–3949.

Willemsen, B., A. Malcolm, and W. Lewis, 2016, A numerically exact local solver applied to salt boundary inversion in seismic full-waveform inversion: Geophysical Journal International, **204**, 1703–1720.

Yee, K. S., 1966, Numerical solution of initial boundary value problems involving Maxwell's equations in isotropic media: IEEE Transactions on Antennas and Propagation, **14**, 302–307.